International Journal of Chemical Studies

P-ISSN: 2349–8528
E-ISSN: 2321–4902
IJCS 2019; 7(4): 1877-1881

Received: 25-05-2019
Accepted: 27-06-2019

Ashis K Sarker
Department of Chemistry, Mawlana Bhashani Science and Technology University, Santosh, Tangail Bangladesh

Correspondence
Ashis K Sarker
Department of Chemistry, Mawlana Bhashani Science and Technology University, Santosh, Tangail Bangladesh

Synthesis of p-type small molecule hole transport material for colloidal quantum dot solar cells

Ashis K Sarker

Abstract
We designed and synthesized a acceptor-donor-acceptor (A-D-A) structured conjugated small molecules, 7, 7'- ((4,8-bis((2-ethylhexyl)oxy)benzo [1,2-b:4,5-b'] dithiophene-2, 6-diyl) bis (4 octylthiophene-5, 2-diyl)) bis (4-(4-octylthiophen-2-yl) benzo [c] [1,2,5] thiadiazole) (BDTTBT), and applied as hole transport layer (HTL) for colloidal quantum dot solar cells (CQDSCs). The BDTTBT based device achieved the highest PCE (8.47%) among the reported CQDSCs using SM HTLs, and also higher than the conventional P3HT based devices (7.60%).

Keywords: Colloidal, rectification, extraction, photon, quantum dot

Introduction
Colloidal quantum dot (CQD) based solar cell (CQDSC) devices have received attention as one of promising next-generation solar cells due to their peculiar properties such as solution-processibility at low temperature, size-dependent bandgap tuning, and multiple exciton generation [1, 2]. Recently, the power conversion efficiency (PCE) of CQDSC reached up to 11.3% through the surface trap density control PbS CQDs [3]. The architecture of CQDSCs also have been developed in the ways to improve charge generation and extraction. The interfacial charge transfer at electron transport layers (ETLs)/CQD interface and CQD/hole transport layers (HTLs) interface has been a crucial factor to determine charge collection properties of devices [4-6]. Most of reported high-efficiency devices have a device architecture, in which iodide-capped CQDs are used as light absorbing active layers, while n-type wide bandgap metal oxides (TiO_2, ZnO etc.) and p-type CQDs (p-CQD) are used as ETL and HTL respectively. In this structure, the rectification occurs at both ETL/CQD and CQD/HTL junctions to augment internal electric field improving charge extraction [5]. While the charge extraction improvement in devices through the modification of metal oxide based ETLs has been widely reported [7-11], the studies on the development of HTL materials has been limited. Considered that the near infrared (NIR) photon to current conversion in devices occurs majorly at rear-side CQD/HTL, the development of HTLs are essential agenda. Thus far, p-CQDs such as 1,2-ethanedithiol (EDT) or 3-mercaptopropionic acid (MPA) capped PbS CQDs has been the best performing HTL and almost exclusively used in high-efficiency devices [3, 5, 12]. However, the preparation of p-CQD HTLs typically contained the solid-state-exchange (SSE) step which is not compatible to high throughput processing techniques.
Organic p-type polymers such as poly(3-hexylthiophene) (P3HT) has employed as HTL to replacing p-CQD HTLs [13, 14]. In the previously reported devices using P3HT as HTL, the PCEs of 5.1% [13] and 7.5% [14] were was achieved using MPA-capped PbS CQD and iodide-capped PbS CQD as active layers respectively. Organic p-type small molecules (SM) were also employed as HTLs for CQDSCs. 2,2',7,7'-tetrakis(N,N-di-pmethoxyphenilamine)-9,9'-spirobifluorene (spiro-OMeTAD), which is the most reputed HTL material for perovskite solar cells, used as SM HTL for CQDSCs, however only disappointing PCE of 0.49% was obtained [13]. Another spiro(fluorene-9,9′-xanthene) containing SM, BTPA-4, was recently reported as HTL for CQDSCs achieving PCE of 5.55% [15]. Based on the PCEs of the reported devices using SM HTLs, the performance of SM HTLs were considerably lower than those of polymer HTL, P3HT, and p-CQD HTLs. Counting the advantages of SMs over polymers such as confirmed molecular weight, low batch-to-batch derivation, and easier purification, the development of new SM HTLs can provide chance for further performance improvement of organic HTLs for CQDSCs.

In this work, we synthesized a acceptor-donor-acceptor (A-D-A) structured conjugated SM,7,7'-((4,8-bis((2-ethylhexyl) oxy) benzo [1, 2-b: 4, 5-b'] dithiophene-2, 6-diyl) bis (4 octylthiophene-5, 2-diyl)) bis (4-(4-octylthiophen-2-yl)benzo [c] [1, 2, 5] thiadiazole) (BDTTBT), and applied as HTL for CQDSCs. The co-existence of D and A in the structure yielded appropriate energy levels for the charge transfer from CQD active layers. While the sufficiently high lowest unoccupied molecular orbital (LUMO) energy level can block the electrons from CQDs, the weak electron donating benzo [1,2-b:4,5-b'] dithiophene (BDT) moiety yielded lower highest occupied molecular orbital (HOMO) energy level than P3HT. Moreover, the alternation of D and A effectively stabilizes the quinoidal structure of BDTTBT, which enhances backbone planarity, thus the molecular packing and hole transport were improved. The CQDSC using BDTTBT exhibited superior performance to that using P3HT due to enhanced charge transfer and declined charge recombination. The BDTTBT based device achieved the highest PCE (8.47%) among the reported CQDSCs using SM HTLs, and also higher than the conventional P3HT based devices (7.60%). In the view point of engineering, our BDTTBT based device used CQD ink as the active layers, thus the entire device fabrication was completed without SSE steps.

Experimental Section

Materials: All the reactions and manipulations were carried out under nitrogen atmosphere with the use of standard Schlenk techniques. All the materials were commercially available and used as received unless specified. Chloroform was dried over CaH_2 and freshly distilled prior to use. Two important intermediates 4,7-bis(4-octylthiophene-2-yl)benzo [c] [1, 2, 5] thiadiazole(TBT) and 2,6-bis(trimethyltin)-4,8-bis(2-ethylethoxy) benzo [1, 2-b:4, 5-b'] dithiophene (BDT) were prepared according to the literature. The detail procedures were described below.

Synthesis of2-(4-octyl-2-thienyl)-4,4,5,5-tetramethyl-1,3,2-dioxaborolane: 3-otylthiopene(4.9g, 0.025mmol, 5.38ml) was dissolved in tetrahydrofuran (THF) (50ml) and cooled -78°C using dry ice and acetone mixture. And 12.5ml of lithium diisopropylamide (0.025mmol 2.0M in Hexanes and THF) was added into flask dropwise. The reaction mixture was then stirring for 2.5h. Subsequently trimethylborate was added drop wise and stirred at –78°C for 1.5h. The reaction mixture was warmed to 25°C and HCl solution was added. The reaction mixture was stirred for 1.5h. The mixture was extracted with diethyl ether, dried over anhydrous $MgSO_4$, and the solvent was removed to afford the intermediate boronic acid as a semi-solid. The boronic acid was dissolved in dry toluene (60ml) and refluxed for 18h in pinacol (2.95g, 0.025mmol) using Dean-Stark trap. The mixture was evaporated to afford the crude product as a deep orange color liquid. The crude product was purified by column chromatography on silica gal using a mixture of dichloromethane and hexane (1:1) as eluent. (2.3g yield 30%).^{1}H NMR ($CDCl_3$, 400MHz) σ = (ppm :) 7.48(s, 1H) 7.21(s, 1H) 2.62(t, 2H) 1.61(m, 2H) 1.28(m, 10H) 0.88(t, 3H).MS (LC-Mass): $[M+H]^+$, 323.2m/z.

Synthesis of 4, 7-bis (4-octyl-2thienyl)-2, 1, 3-benzothiadiazole (TBT): 2-(4-octyl-2-thienyl)-4, 4, 5, 5-tetramethy l-1, 3, 2-dioxaborolane (3.22g, 10mmol), 4, 7-dibromo-2, 1, 3-benzothiadiazole (1.18g, 4mmol), and 5 mol % of tetrakis-(triphenylphosphine) palladium [Pd (PPh_3)$_4$] (460mg) were dissolved in THF (60ml) and stirred for 30 min. Potassium carbonate (K_2CO_3) (3.31g, 24mmol) was dissolved in H_2O (5ml), degassed, and added to the mixture. The mixture was refluxed for 52h. The mixture was extracted with dichloromethane, the organic phase was dried over anhydrous $MgSO_4$, and the solvent was removed to afford the product as a red solid. The crude product was purified by column chromatography on silica gel using a mixture of dichloromethane and hexane (7:3) as eluent. (1.41g, yield 66%). ^{1}H NMR ($CDCl_3$, 400MHz) σ = (ppm :) 7.98(s, 2H) 7.82 (s, 2H) 7.04 (s, 2H) 2.69 (t, 4H) 1.70 (m, 4H) 1.32 (m, 20H) 0.88 (t, 6H). ^{13}C NMR ($CDCl_3$) σ = 152.63, 144.38, 139.01, 129.01, 126.01, 125.53, 121.53, 31.92, 30.68, 30.54, 29.49, 29.32, 22.71, 14.14 ppm. MS (LC-Mass): $[M+H]^+$, 525.2m/z.

Synthesis of BrTBT: N-Bromosuccinimide (0.17 g, 0.96 mmol) was added in a small portions to a solution of TBT (0.4724 g, 0.90 mmol) in chloroform and acetic acid (40 mL, 3:1, v/v) at 0°C. After being stirred overnight at room temperature, the reaction mixture was poured into water and extracted with CH_2Cl_2. The organic layer was thoroughly washed twice with water, Na_2CO_3 and then dried over $MgSO_4$. After removal of solvent it was chromatographed on silica gel using a mixture of Hexane and Chloroform (4:1) as eluent to afford BrTBT (0.47 g, 87.04%) as a red solid.^{1}H NMR (400 MHz, CDCl3): δ 8.00 (s, 1H), 7.83 (d, 1H), 7.78 (s, 1H) 7.77 (d, 1H), 7.0 (s, 1H), 2.64 (m, 4H),) 1.78 (m, 2H) 1.69 (m, 2H) 1.30-1.45 (m, 20H) 0.88 (m, 6H).^{13}C NMR ($CDCl_3$) σ :152.43; 152.26; 144.41; 142.96; 138.85; 138.64; 129.17; 127.83; 126.24; 125.27; 124.87; 124.85; 121.70; 111.36; 31.94; 31.63; 30.68; 30.54; 29.83; 29.76; 29.71; 29.52; 29.46; 29.35; 29.33; 22.73; 22.70; 14.17. MS (MALDI-TOF): m/z: 604.314 [M^+]; $C_{30}H_{39}N_2S_3Br$ (603.74).

Synthesis of BDTTBT: Solid BrTBT (0.3478 g, 0.58 mmol) and BDT (0.216 g, 0.28 mmol) were dissolve in toluene (50 mL) and transferred into vacuum dried three necked flask using cannula. Bis(triphenylphosphine)palladium(0) (11.56 mg, 4 mol% of BDT unit) was poured to the reaction vessel and refluxed for 50 h using oil bath, the reaction mixture was poured into water and extracted with chloroform. The organic layer was washed with water, Na_2CO_3 and then dried over $MgSO_4$. After removal of solvent it was chromatographed on silica gel using a mixture of hexane and chloroform (4:1) as eluent to afford BDTTBT (0.35 g, 85.0%) as a black solid.^{1}H NMR (400 MHz, $CDCl_3$): δ 8.05 (s, 2H), 8.01 (s, 2H), 7.87 (dd, 4H), 7.58 (s, 2H), 7.06 (s, 2H), 4.25 (d, 4H), 2.99 (t, 4H), 2.71 (t, 4H), 1.80 (m, 6H), 1.69 (m, 6H), 1.26-1.49 (m, 48H), 1.08 (t, 6H), 0.99 (t, 6H), 0.86 (m, 12H).^{13}C NMR ($CDCl_3$) σ : 152.52; 152.50; 144.40; 143.98; 141.80; 138.96; 138.04; 135.74; 132.39; 132.01; 130.91; 129.72; 129.11; 126.21; 125.39; 125.13; 121.67; 118.27; 40.73; 31.97; 30.79; 30.68; 30.55; 29.86; 29.63; 29.51; 29.45; 29.35; 23.93; 23.25; 22.74; 14.31; 14.16; 11.44. MS (MALDI-TOF): m/z: 1492.373 [M^+]; $C_{86}H_{114}N_4O_2S_8$ (1492.37).

Characterization: The ^{1}H and ^{13}C NMR spectra were recorded on a Bruker AV400 Spectrometer. UV/Vis spectra were obtained with a JASCO V-570 spectrophotometer. Cyclic voltammetry (CV) experiments were performed with a LK98B II microcomputer-based electrochemical analyzer. All CV measurements were carried out at room temperature with a conventional three-electrode configuration employing a glassy carbon electrode as the working electrode, a saturated

calomel electrode (SCE) as the reference electrode, and a Pt wire as the counter electrode. Dichloromethane was distilled from calcium hydride under dry nitrogen immediately prior to use. Tetrabutylammonium phosphorus hexafluoride (Bu_4NPF_6, 0.1 M) in dichloromethane was used as the supporting electrolyte, and the scan rate was 50 mV s^{-1}.

Device fabrication: The CQDSC devices were fabricated using the BDTTBT as HTL (Figure 1). First, ~40 nm-thick ZnO ETLs were prepared on indium-doped tin oxide (ITO) deposited glass substrates by in-situ sol-gel conversion at 130 °C [9,16]. The CQD active layers were fabricated by direct spin-coating of iodide-capped CQD ink on ZnO-ETLs at room temperature followed by drying [16]. During the deposition of CQD active layers, no additional steps such as SSE or LbL deposition were used. The organic HTLs (BDTTBT or P3HT) were also spin-coated on the CQD active layers at room temperature. The P3HT based device was also fabricated by identical fabrication procedure. For anode, MoOx/Ag (10 nm/100 nm) layers were thermally deposited at reduced pressure (~10^{-6} torr). We used thin MoOx layer between organic HTLs and Ag in order to decouple from any unwanted surface issues in both HTMs such as pin-hole formation, in addition to more effective electron blocking [17-20].

Results and Discussion

Synthesis and Characterization of BDTTBT

Boronic esters are very useful synthetic intermediates because it can be converted into a broad range of functional groups, often with complete stereo specificity. Therefore, 2-(4-octyl-2-thienyl)-4, 4, 5, 5-tetramethyl-1, 3, 2-dioxaborolane was synthesized by lithiation-borylation reaction with LDA (lithium diisopropylamide) and trimethyl borate, followed by esterification using pinacol. The synthesis of 4,7-bis(4-octyl-2thienyl)-2,1,3-banzothiazole was performed via Suzuki coupling reaction with 4,7-dibromo-2,1,3-benzothiadiazole. After bromination, the final molecule, BDTTBT was achieved using Stille coupling reaction with 2,6-Bis(trimethylstannyl)-4, 8-bis (2-ethylhexyloxy) benzo [1,2-*b*:4,5-*b*′] dithiophene. The synthetic procedures of the SM, BDTTBT, is shown in Scheme 1. Two electron accepting TBT units were conjugated with a weak electron-donating BDT core. The structural characterization results for BDTTBT are shown in the Supporting Information (SI).

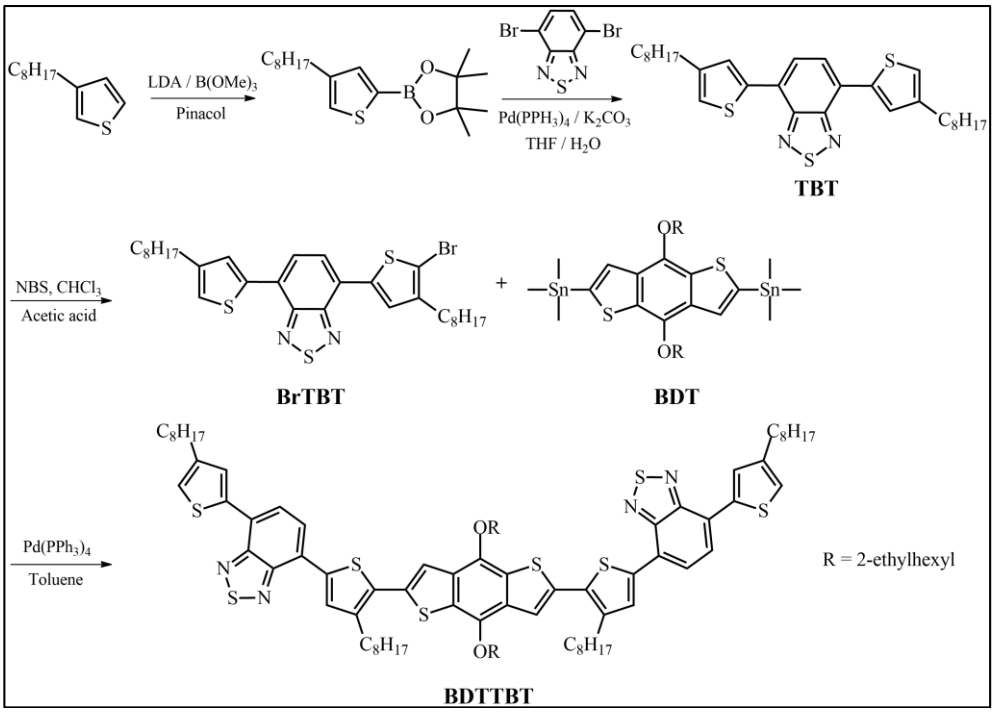

Scheme 1: The synthetic route to BDTTBT

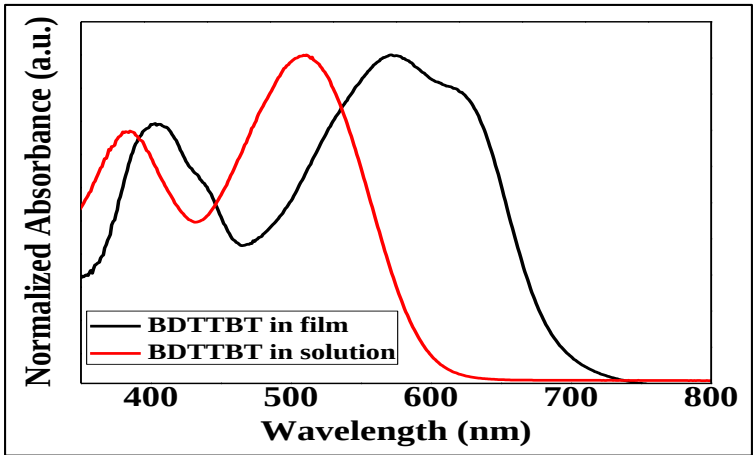

Fig 1: UV/Visible absorption spectra of BDTTBT in solution and film state.

Optical Properties: Ultraviolet-visible **(**UV-Vis) spectra of BDTTBT, both solution and film samples, are shown in Figure 1. The absorption peak of BDTTBT film was red-shifted by ~53 nm compared to its solution spectra with clear vibronic shoulder, which indicates the effective backbone π-π packing in film state. The optical bandgap of BDTTBT was estimated from the onset absorption of film sample was 1.78 eV (Figure 1 and Table 1). The energy levels of CQD active layer and BDTTBT, and P3HT were also determined by ultraviolet photoelectron spectroscopy (UPS) analysis, and the results are shown in Figure 2.

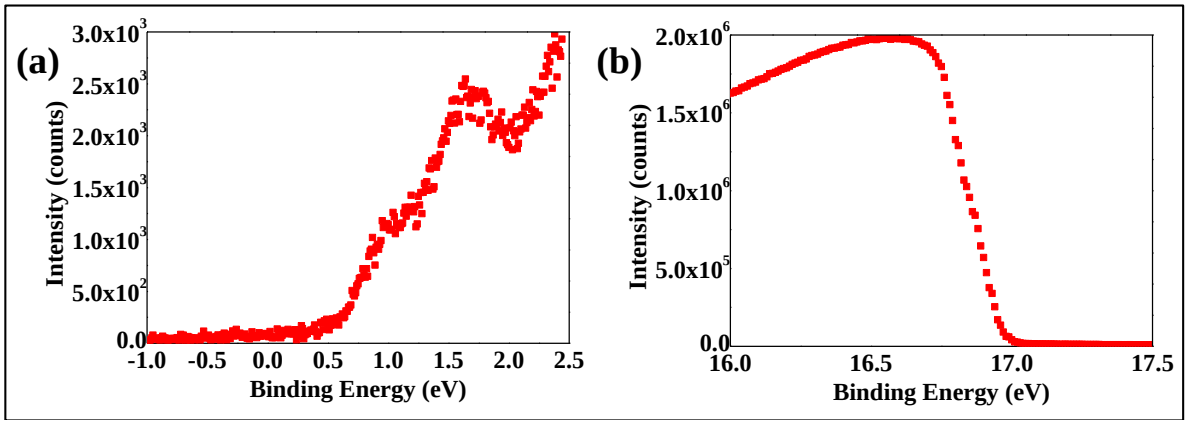

Fig 2: UPS spectra of BDTTBT for (a) valence band region, (b) secondary electron cut-off region

The HOMO values were determined using the Fermi-level values from the secondary electron cut-off region, and the valence band edges relative to Fermi-level obtained from the onset of low binding energy region. The LUMO levels were determined using optical bandgaps from UV-vis spectra. The energy levels of CQD and HTMs were summarized in Table 1. The energy levels of BDTTBT and P3HT were appropriate to extract holes, while the LUMO levels of them were sufficiently high to block electron back transfer. The lower-lying HOMO and Fermi levels of BDTTBT than P3HT is more favorable for hole extraction from CQD layers and higher open circuit voltage (V_{OC}) the device. The electrochemical bandgap of BDTTBT was determined to be 1.81 eV, which is also in a good agreement with the optical bandgap (Figure 3). The results from UV-vis spectra of BDTTBT were summarized in Table 1.

Table 1: Summary of characteristics of HTL.

HTL	E_g^{opt} (eV)	E_{HOMO} (Ev)	E_{Fermi} (eV)	E_{LUMO} (eV)
BDTTBT	1.79	-4.81	-4.24	-3.02
P3HT	1.89	-4.60	-4.10	-2.71

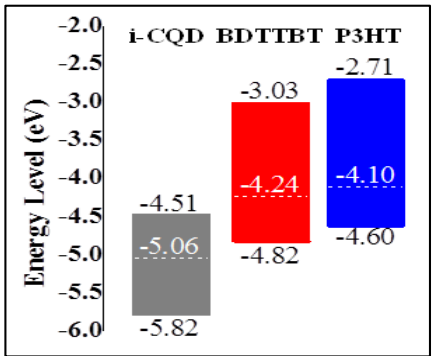

Fig 3: Estimated energy level of CQD.

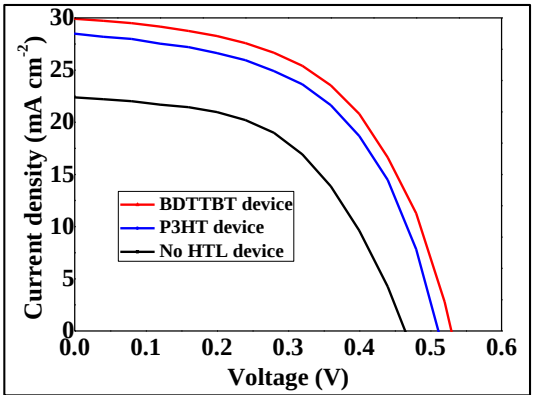

Fig 4: Current density−voltage (J−V) curves.

Photovoltaic Properties. Figure 4 shows the current density-voltage (*J*-*V*) characteristics of the devices using BDTTBT as HTL under AM 1.5G one sun illumination. The PCE of device without HTL was 5.41%with V_{OC} of 0.46 V (Figure 4 and Table 2). When organic HTMs were inserted between CQD layer and anode, the performance was substantially improved. The BDTTBT based device exhibited the PCE of 8.47% with V_{OC} of 0.53 V, short-circuit-current-density (J_{SC}) of 29.91 $mAcm^{-2}$, and fill factor (FF) of 0.53, while the P3HT device based showed PCE of 7.78% with V_{OC} of 0.51 V, J_{SC} of 28.48 $mAcm^{-2}$, and FF of 0.53. Table 2 shows the summery of average device parameters obtained from 30 devices for each, which confirms the consistency in device performance. Notably, the BDTTBT device achieved superior PCE to P3HT device mainly due to the boosted V_{OC} in BDTTBT device. We attribute the enhanced V_{bi} in BDTTBT device to the lower-lying HOMO energy level of BDTTBT (-4.82 eV) than P3HT (-4.60 eV). The higher V_{bi} in BDTTBT based device is responsible for the increase in V_{OC} (~0.03 eV) compared to P3HT device.

Table 2: Summary of device performances

Device	PCE (%)	V_{OC} (V)	J_{SC} (mA/cm^2)	FF
With BDTTBT	7.72	0.53	26.91	0.54
With P3HT	6.94	0.49	25.28	0.56
Without HTL	4.54	0.42	21.19	0.52

Conclusion

The PCE of device without HTL was 5.41%with V_{OC} of 0.46 V. When organic HTMs were inserted between CQD layer and anode, the performance was substantially improved. The BDTTBT based device exhibited the PCE of 8.47% with V_{OC} of 0.53 V, short-circuit-current-density (J_{SC}) of 29.91 $mAcm^2$, and fill factor (FF) of 0.53, while the P3HT device based showed PCE of 7.78% with V_{OC} of 0.51 V, J_{SC} of 28.48 $mAcm^{-2}$, and FF of 0.53. The V_{OC} of BDTTBT device (0.53V) was higher than that of P3HT device (0.51 V) due to the increased rectification.

Acknowledgement

This work was supported by Kookmin University, Seoul, South Korea and Mawlana Bhashani Science and Technology University, Santosh, Tangail-1902, Bangladesh.

Conflicts of Interest

The author declares that there are no conflicts of interest related of this article.

ORCID ID: https://orcid.org/0000-0002-5054-9152

References

1. Semonin OE *et al*. Peak External Photocurrent Quantum Efficiency Exceeding 100% via MEG in a Quantum Dot Solar Cell. Science. 2011; 334(6062):1530-1533.
2. McDonald SA *et al*. Solution-processed PbS quantum dot infrared photodetectors and photovoltaics. Nature Materials. 2005; 4(2):138-U14.
3. Liu M *et al*. Hybrid organic-inorganic inks flatten the energy landscape in colloidal quantum dot solids. Nature Materials. 2016; 16(2):258-263.
4. Pattantyus-Abraham AG *et al*. Depleted-Heterojunction Colloidal Quantum Dot Solar Cells. Acs Nano. 2010; 4(6):3374-3380.
5. Chuang CHM *et al*. Improved performance and stability in quantum dot solar cells through band alignment engineering. Nature Materials. 2014; 13(8):796-801.
6. Ko DK *et al*. p-i-n Heterojunction Solar Cells with a Colloidal Quantum-Dot Absorber Layer. Advanced Materials. 2014; 26(28):4845-4850.
7. Azmi R, SH Oh, SY Jang. High-Efficiency Colloidal Quantum Dot Photovoltaic Devices Using Chemically Modified Heterojunctions. ACS Energy Letters. 2016; 1(1):100-106.
8. Azmi R *et al*. Improved performance of colloidal quantum dot solar cells using high-electric-dipole self-assembled layers. Nano Energy. 2017; 39:355-362.
9. Azmi R *et al*. Low-Temperature-Processed 9% Colloidal Quantum Dot Photovoltaic Devices through Interfacial Management of p-n Heterojunction. Advanced Energy Materials, 2016.
10. Liu M *et al*. Double-Sided Junctions Enable High-Performance Colloidal - Quantum - Dot Photovoltaics. Advanced Materials. 2016; 28(21):4142-4148.
11. Kim GH *et al*. High-Efficiency Colloidal Quantum Dot Photovoltaics via Robust Self-Assembled Monolayers. Nano Letters. 2015; 15(11):7691-7696.
12. Choi J *et al*. Chloride passivation of ZnO electrodes improves charge extraction in colloidal quantum dot photovoltaics. Advanced, 2017.
13. Zhang X *et al*. Slow recombination in quantum dot solid solar cell using p-i-n architecture with organic p-type hole transport material. Journal of Materials Chemistry A. 2015; 3(41):20579-20585.
14. Neo DCJ *et al*. Poly (3-hexylthiophene-2, 5-diyl) as a Hole Transport Layer for Colloidal Quantum Dot Solar Cells. ACS Applied Materials & Interfaces. 2016; 8(19):12101-12108.
15. Zhang Y *et al*. Improvement of Photovoltaic Performance of Colloidal Quantum Dot Solar Cells Using Organic Small Molecule as Hole-Selective Layer. The Journal of Physical Chemistry Letters, 2017.
16. Aqoma H *et al*. High-Efficiency Photovoltaic Devices using Trap-Controlled Quantum-Dot Ink prepared via Phase-Transfer Exchange. Advanced materials (Deerfield Beach, Fla.), 2017.
17. Speirs MJ *et al*. Temperature dependent behaviour of lead sulfide quantum dot solar cells and films. Energy & Environmental Science. 2016; 9(9):2916-2924.
18. Speirs MJ *et al*. Increased efficiency in pn-junction PbS QD solar cells via NaHS treatment of the p-type layer. Applied Physics Letters. 2017; 110(10):103904.
19. Kim J *et al*. Efficient planar-heterojunction perovskite solar cells achieved via interfacial modification of a sol–gel ZnO electron collection layer. Journal of Materials Chemistry A. 2014; 2(41):17291-17296.
20. Gao J *et al*. n-Type Transition Metal Oxide as a Hole Extraction Layer in PbS Quantum Dot Solar Cells. Nano Letters. 2011; 11(8):3263-3266.